Proceedings 10th NUMGE 2023
10th European Conference on Numerical Methods in Geotechnical Engineering
Zdravkovic L, Kontoe S, Taborda DMG, Tsiampousi A (eds)

https://doi.org/10.53243/NUMGE2023-65

A new strategy for the initialization of MPM simulations

M. Lu[1], V. Girardi[2], M. Zhou[1], F. Ceccato[2]

[1] *Department of Geotechnical Engineering, Tongji University, Shanghai, PRC*
[2] *Department of Civil Environmental and Architectural Engineering, University of Padua, Padova, Italy*

ABSTRACT: Material point methods (MPM) are widely used to tackle large displacement problems in geotechnical engineering. However, current multiphase MPM formulations are mainly implemented on the basis of explicit time integration schemes and are inefficient for simulating long time processes, such as the consolidation and seepage in saturated and unsaturated soils. To improve that, this study proposes a new strategy for the initialization of MPM simulations, where kernel interpolation is used to map the previously derived field variables (e.g., soil properties, pore pressure, stress and strain) to the material points of the model for the large deformation analysis. These field variables can be the results with a generic distribution obtained from model experiments, in-situ tests, or numerical simulations. Two typical kernel functions, i.e., the cubic spline and Gaussian functions, are used for the mapping procedure. Parametric analysis indicates that the smoothing length of kernel functions highly depends on the distribution of field variables. The proposed strategy is applied to investigate the runout behavior of an instrumented slope failure caused by artificial rainfall. It shows a good agreement between results obtained from the strategy and the experiment.

Keywords: Material point method; initialization; computational efficiency; mapping procedure; kernel interpolation

1 INTRODUCTION

In the past decades, mesh-based and mesh-free numerical techniques have been developed to solve large displacement problems in geotechnical engineering (Soga et al., 2016), such as Arbitrary Lagrangian Eulerian, Coupled Eulerian Lagrangian, Discrete Element Methods, Material Point Methods, Smooth Particle Hydrodynamics, and Particle Finite Element Method. These methods overcome the limitations of traditional Lagrangian finite element method (FEM) applied in computational geomechanics, which are very well suited for small deformation problems but fail to simulate large displacement because of issues with element distortions.

In this paper, the material point method (MPM) is used. It was first developed by Sulsky et al. (1994) for one-phase material in solid mechanics, and it has been significantly improved since then and largely applied in geomechanics (Fern et al. 2019). The material body is discretized with a set of material points (MPs) which carry all information (e.g., kinematic variables, stresses, soil properties and state variables), and the problem domain is covered by the background mesh. The balance equations are solved on the background mesh and used to update the information on the MPs. Large deformations are simulated with MPs moving through the mesh.

In recent years, many researchers have extended MPM to multiphase materials; see, e.g. Bandara et al., 2016; Wang et al., 2018; Ceccato et al., 2021, among others, which provide useful insights to solve saturated and unsaturated soil problems based on MPM. However, most of the available multiphase MPM formulations are dynamic, in which explicit time discretization algorithms are applied (Yerro et al., 2022). Such algorithms usually require small time increments to ensure the numerical stability. Thus, current MPM formulations are proper to simulate fast dynamic processes, but inefficient to handle long time processes, such as consolidation and infiltration.

In order to exploit the potentialities of these numerical tools, a new strategy for the initialization of the MPM simulations is proposed. The strategy consists of generating the initial conditions of the MPM analysis with a more efficient method and using a interpolation algorithm to map a generic spatial distribution of field variables (e.g., porosity, pore pressure, stress, and strain) from this previous analysis to MPs for the subsequent dynamic large displacement analysis. The mapping procedure is explained and validated in Sec. 2. The advantage of this algorithm is its wide applicability to different variables and spatial distribution; indeed, field variables can be obtained in different ways, such as numerical analyses, model experiments, and in-situ tests.

In this paper, the proposed strategy is applied to the simulation of an experimental rainfall-induced landslide in Sec. 3. The triggering phase, during which infiltration occurs with small displacement, is simulated with FEM (Sec. 3.1), then pressure and total stresses are mapped to MPM for the simulation of the fast collapse phase

(Sec. 3.2). The displacements obtained numerically are compared with the experimental evidences.

2 A NEW INITIALIZATION STRATEGY

The key of the proposed strategy is to map field variables with a spatial distribution to the initial position of material points (MPs), which can be carried out on the basis of interpolation tecniques. In the literature, spatial interpolation is generally divided into two categories (Lam, 1983), namely, exact (e.g., kriging and spline interpolation) and approximate models (e.g., tension finite difference, inverse distance weighting and kernel interpolation). In this study, the kernel interpolation is used since it has the simplest parameter and reliable prediction performance. Moreover, as indicated in parametric analysis, which will be shown later, the parameter of the kernel interpolation has a good relationship with the distribution of field variables for ease of application.

The principle of the kernel interpolation is to make a prediction at an unknown point according to observed points close to the unknown point. More weights are given to an observed point which has a shorter distance from the unknown point (Mühlenstädt and Kuhnt, 2011). The weight function is indeed called the kernel function, denoted as w. The kernel interpolation can be written using the following equation:

$$f\left(x,h\right)=\frac{\sum_{i=1}^{m}\left[w\left(\frac{d_i}{h}\right)f\left(x_i\right)\right]}{\sum_{i=1}^{m}w\left(\frac{d_i}{h}\right)} \tag{1}$$

in which $f(x, h)$ is an unknown funcion at point x; $f(x_i)$ is the funcions observed at point x_i; d_i is the actual distance between x and x_i; h is the smoothing length; and m is the number of observed points.

Many kernel functions have been developed. Particularly, the cubic spline and Gaussian functions are most widely used. Let R denote d_i/h. The cubic spline function can be expressed using the following equation (Monaghan and Lattanzio, 1985):

$$w\left(R\right)=\alpha\times\begin{cases}2/3-R^2+R^3/2, & 0\le R<1\\ \left(2-R\right)^3/6, & 1\le R<2\\ 0, & R\ge 2\end{cases} \tag{2}$$

in which the values of α for one, two, three-dimensional space adopt, repectively, $1/h$, $15/7\pi h^2$, and $3/2\pi h^3$ for the unity requirement. It can be seen from Eq. (2) that when distances between observed points and unknown points are longer than two times of smoothing length, the data at these observed points are not used for the prediction. On the other hand, the Gaussian function can consider all observed points for the prediction, which can be written as follows (Gingold and Monaghan, 1977):

$$w\left(R\right)=\alpha\times e^{-R^2} \tag{3}$$

where in one, two, and three-dimensional space, $\alpha = 1/\pi^{1/2}h$, $1/\pi h^2$, and $1/\pi^{3/2}h^3$, respectively. In the next section, these two kernel functions are both examined for the mapping procedure.

The above technique has been incorporated into the in-house version of the open-source MPM software Anura3D (www.anura3d. com).

2.1 Calibration and performance evaluation

As an illustration, consider a finite element model of a square block with the size of 50 × 50 m, which is shown in Fig. 1(a). The triangular mesh is used and the mesh size is 5 m. Zero pore pressure is applied to the upper side of the block, and the other sides are impermeable. After the steady-state analysis conducted with the commercial FEM software SEEP/W of Geostudio, the pore pressure distribution of the block is derived as shown in Fig. 1(b). It suggests that the pore pressure linearly increases with the depth. The task here is to build the kernel interpolation model based on the pore pressure of the block.

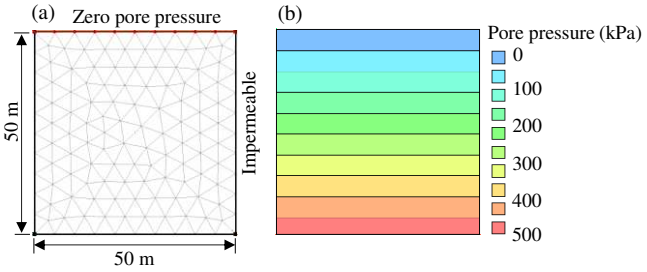

Figure 1. (a) Geometry, discretization, and boundary conditions of a square block based on the FEM. (b) Pore pressure distribution of the square block based on the FEM model

There are 135 mesh nodes in the finite element model, thus 135 data points of pore pressure are first extracted. Then, these points are divided into two parts, that is, 1 and 134 points. The 134 data points are used to predict the 1 data point, i.e., m = 134 in Eq. (1). The smoothing length h can be calibrated through minimizing the error between the prediction and the observation as follows:

$$h\leftarrow\min\sum_{j=1}^{n}\left|f\left(x_j\right)-f\left(x_j,h\right)\right| \tag{4}$$

where $f(x_j)$ is the pore pressure at x_j observed from the finite element model; $f(x_j, h)$ is the pore prssure at x_j predicted on the basis of the other 134 points using Eq. (1); and n is the number of predictions. In this example, n = 135 as all data points are used to be predicted.

Eventually, Eq. (4) is solved with the simulated annealing algorithm (Henderson et al., 2003). The smoothing lengths of cubic spline and Gaussian kernel functions are respectively 5.07 and 4.17 m.

To evaluate the prediction performance of kernel interpolation, the mesh size of the finite element model is changed to 3 m, and the pore pressure of the block at new points is observed. Then, the pore pressures at these new points are predicted on the basis of the kernel interpolation, respectively, with cubic spline and Gaussian functions. Fig. 2 compares the pore pressure of the block predicted by the kernel interpolation and observed from the FEM model. It suggests that the coefficients of determination R^2 between these two results are 0.99, indicating that the kernel interpolation with the cubic spline and Gaussian functions both has the high prediction accuracy.

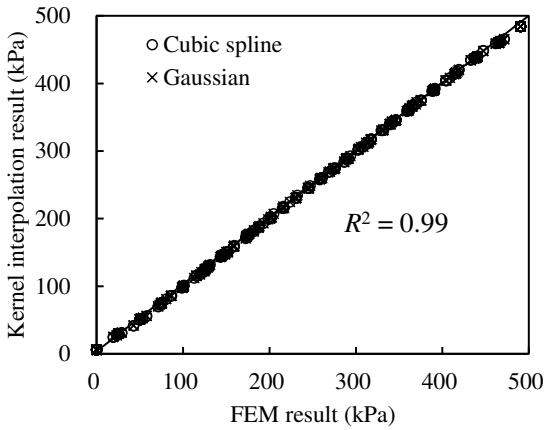

Figure 2. Comparison of pore pressures predicted based on the kernel interpolation and FEM analysis

2.2 Effect of the mesh size

The effect of mesh size on the kernel interpolation is investigated in this section. The same example of the previous section is considered. First of all, the mesh size is a significant factor to influence the distribution of data points. Using the calibration method illustarted in the above subsection, Fig. 3 shows the variation of smoothing lengths of cubic spline and Gaussian functions as the triangular mesh sizes are, respectively, 0.1, 0.5, 1, 5, and 10 m. It is interesting to observe that the optimal smoothing length linearly increases as the triangular mesh size increases. The smoothing length in the cubic spline function is roughly equal to the triangular mesh size, and the smoothing length in the Gaussian function is around 80% of the triangular mesh size.

2.3 Effect of the mesh type

In addition to the size of the mesh, the distribution of data points is also influenced by the type of mesh. To solve this problem, the mesh type of the block is changed to the quadrangle. On the basis of Eq. (4), smoothing lengths of cubic spline and Gaussian functions as the quadrangular mesh sizes vary from 0.1 to 10 m, are calculated and the results are shown in Fig. 3. The smoothing length also linearly increases with the quadrangular mesh size. Compared with the triangular mesh, the smoothing length for the quadrangular mesh is smaller. The optimal smoothing length in the cubic spline function is approximately 70% of the quadrangular mesh size, and the smoothing length in the Gaussian function is approximately 25% of the quadrangular mesh size.

Overall, the smoothing length in the kernel interpolation highly depends on the distribution of field variables. When the field variables are derived on the basis of FEM, there is an obviously linear relationship between the smoothing length and the mesh size. According to the result shown in Fig. 3, the optimal smoothing length can be determined based on the mesh size and type. With the cubic spline function, we can consider that the optimal smoothing length is between 0.7l and l, where l is a reference distance between two observed points.

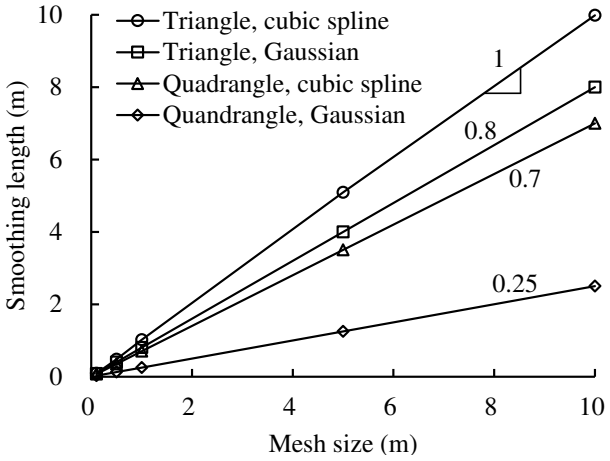

Figure 3. Variation of the smoothing length with mesh size for different mesh types and kernel functions. The number denotes the slope of a line.

3 APPLICATION

In this section, the procedure presented in the previous section is applied to the simulation of an experimental rainfall-induced landslide presented in Lora et al. (2016). As shown in Fig. 4, the model slope is 3.5 m-high, and 6m-long, with the maximum sloping angle of 32°. A layer of loose silty sand with a thickness of 60 cm is placed over a compacted sandy clay. The slope toe consists of a porous wall made of hollow bricks, allowing water to drain from the subsurface (Lora et al., 2016).

Artificial rain with a steady intensity of 150 mm/h was applied on the slope surface until the silty sand layer collapsed. The infiltration process evolved for more than 1.5 h, and the failure occurred suddenly without any warning signs. The collapse duration lasted about 3 seconds. A camera recorded the entire process

and the video was used to determine the displacement field applying the PIV technique (Stanier et al., 2016) of the soil surface, as shown in Fig. 5.

The numerical simulation of this case can be fully performed with the two-phase one-point formulation for unsaturated soil implemented in Anura3D (Ceccato et al. 2021); however, the triggering phase, which lasted about 1.5 h in the experiment, can take several days or weeks to simulate on a desktop computer (Intel processor i7-1165G7 2.80GHz). In contrast, FEM software, e.g., SEEP/W of Geostudio, can simulate it in a few minutes thanks to the use of an implicit time discretization algorithm.

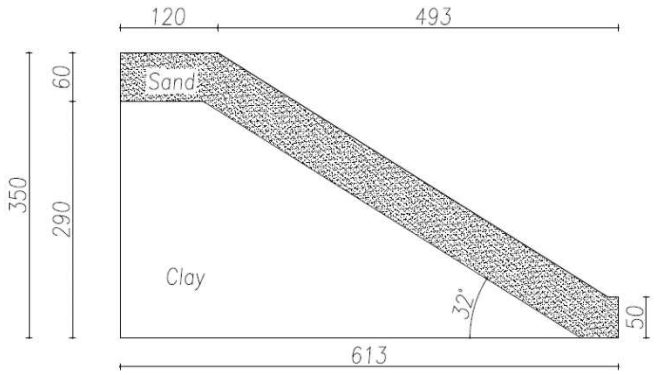

Figure 4. Geometry and soil layers of the experimental model (dimensions in cm)

Figure 5. Final displacements of the experimental model extracted from the video: the black arrows show the directions, and the contour plot the total quantities

For this reason, rainfall infiltration before failure is simulated with a FEM seepage analysis, and then the pore pressure and total stress of the slope at the failure time are mapped into the MPM model for the subsequent large deformation analysis. The failure time is assessed with slope stability analysis.

3.1 FEM analysis

SEEP/W is utilized for transient seepage analysis of the slope under rainfall. The liquid flow in the soil is governed by the Darcy law. The hydraulic constitutive equations adopt the Van Genuchten model (Eq. 5 and 6) (Van Genuchten, 1980):

$$\Theta = \left[\frac{1}{1+\left|\alpha\psi\right|^{n}} \right]^{m} \tag{5}$$

$$k = k_s \sqrt{\Theta} \left[1-\left(1-\Theta^{1/m}\right)^{m} \right]^{2} \tag{6}$$

where Θ is the relative degree of saturation; ψ is the negative pore pressure; k is the hydraulic conductivity; k_s is the saturated conductivity; α, m, n, and l are the fitted parameters, and $m = 1 - 1/n$. Table 1 gives the soil parameter values used in the FEM, which are derived from Lora et al. (2016).

Table 1. Soil parameters in the FEM and MPM models

Soil parameter	**Values**
Solid density (kg/m^3)	2718
Liquid density (kg/m^3)	1000
Young's modulus (kPa)	2500
Poisson's ratio	0.3
Saturated conductivity (m/s)	2.047×10^{-4}
Liquid viscosity (kg/m·s)	1×10^{-3}
Porosity	0.58
Initial degree of saturation	0.31
Liquid bulk modulus (kPa)	4.5×10^{4}
Residual degree of saturation	0.1
Parameters of the Van Genuchten model	$\alpha = 0.51$ $n = 2.73$
Effective cohesion (kPa)	0
Effective friction angle (°)	33
Effective dilatancy angle (°)	0

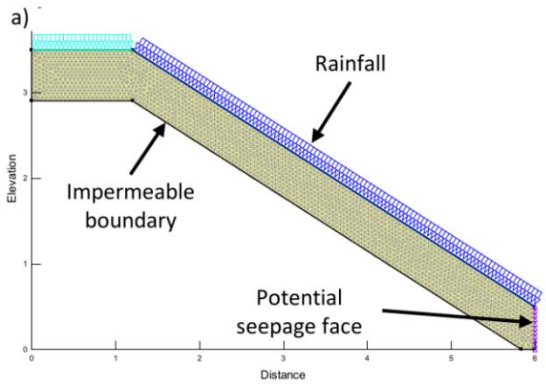

Figure 6. Geometry and discretization of the FEM model

Only the sand layer is simulated and the clay layer is assumed to be an impermeable boundary (Fig. 6). In this model, the bottom and the left side of the slope are impermeable, while the right side is a potential seepage face. A flux equal to 150 mm/h is applied on the slope surface to simulate rainfall infiltration. The triangular mesh is used and the mesh size is 0.05 m. The total number of element nodes is 1829 (Fig. 6).

The transient seepage analysis adopts a time increment of 0.01 h (36 s) and for each step the slope

stability analysis with SLOPE/W is performed to calculate the factor of safety (FS) on the basis of the Mongenstern-Price method (Morgenstern and Price, 1965).

At 1.56 h, FS = 1.009 and this can be considered as the failure time of the slope, which agrees well with the evidence in the experiment. Fig. 7 depicts the critical slip surface and the pore pressure distribution of the slope at the failure time. The total stress of the slope at the failure time is computed with SIGMA/W.

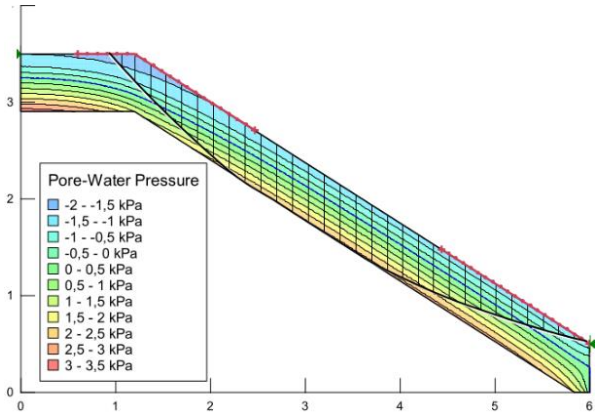

Figure 7. Pore pressure and critical slip surface at the failure time in the FEM model (t = 1.56 h, FS = 1.009)

3.2 MPM analysis

The MPM model of the slope is built with Anura3D as shown in Fig. 8. Its hydraulic boundary conditions are the same as those of the FEM model. Zero solid displacements are prescribed at the bottom boundary, and roller boundary conditions are applied on the lateral surfaces and at the toe of the slope. A triangular computational mesh is used. There are 3 material points in each element of the slope domain. In total, around 1700 computational meshes and 3700 material points are used in the MPM model. Five MPs are monitored for displacement (A-E in Fig. 8).

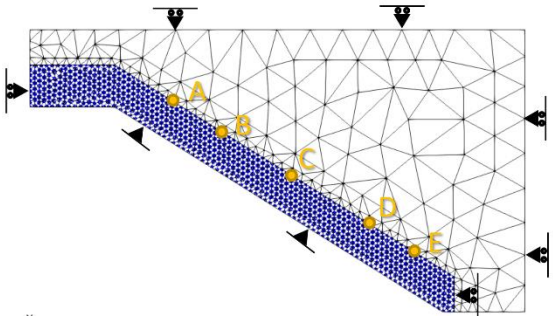

Figure 8. Geometry and discretization of the MPM model

In the MPM model, the effective stress of the slope is calculated based on the Bishop's equation ($\sigma = \sigma' + Sp$, σ = total stress, σ' = effective stress, p = pore pressure, and S = degree of saturation). The mechanical constitutive equations use the elastoplastic model with Mohr-Coulomb failure criterion. The hydraulic constitutive models are identical to the FEM model. The values of soil parameters used in the MPM model are also shown in Table 1 (Lora et al., 2016).

Stresses are initialized with the procedure explained in the previous section and they are depicted in Fig. 9. The cubic spline function is used for the kernel interpolation. First, the pore pressure and total stress are extracted at each element node of the FEM model. There are 1829 data points in total. Based on these points, the smoothing length h is calibrated using Eq. (4), which is equal to 0.046 m, close to the mesh size of 0.05 m. Using Eq. (1), the pore pressure and total stress at the failure time are mapped to the MPs.

Although in reality small displacements in the slope have already occurred before failure, they are neglected and the displacements of MPs at the initial condition are assumed to be zero.

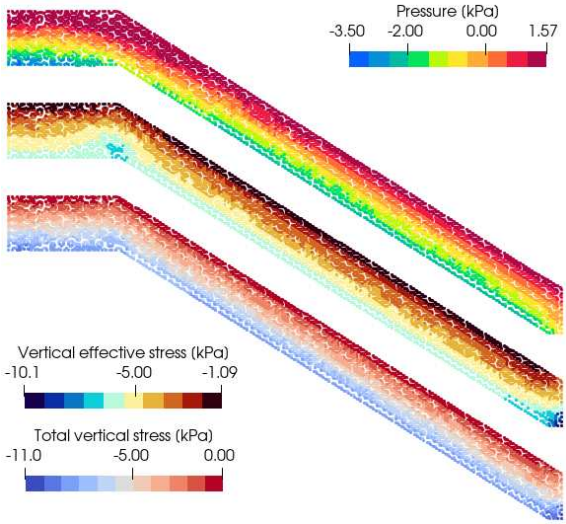

Figure 9. Initial pore pressure (top), effective stress (middle) and total stress (bottom) in the MPM model

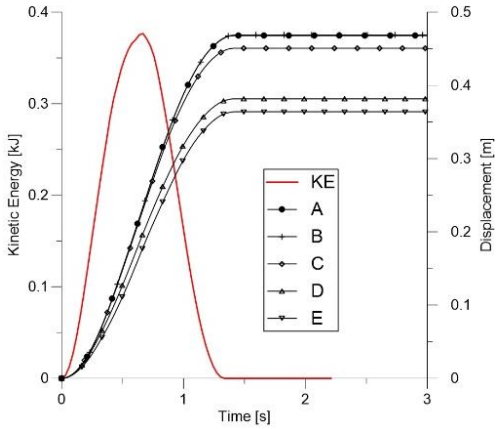

Figure 10. Evolution of Kinetic Energy (KE) and displacement in the MPM model

The results of MPM analysis, show that the slope develops large displacements reaching a new stable configuration in about 1.7 s as presented in Fig. 10 and the magnitude of displacement is in agreement with the

experiment. In Fig. 11(d) the black arrows indicate the experimental displacement obtained from experiment and the numbers below indicate the displacement magnitude, the blue dotted lines indicate the displacement of reference MPs and the numbers in brackets above indicate the magnitude. It can be observed that there is a relatively good agreement between experiment and simulation, proving the validity of the proposed strategy.

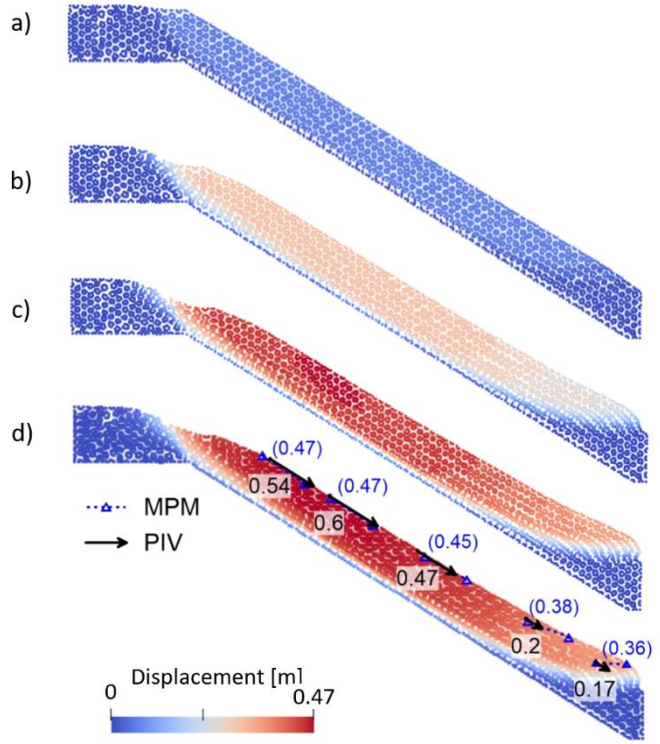

Figure 11. Displacement at different times after failure in the MPM model: (a) 0.3 s, (b) 0.8 s, (c) 1.2 s, (d) 3.0 s

4 CONCLUSION

This study proposes a general and practical strategy for the initialization of MPM simulations to improve computational efficiency. It is a mapping technique implemented based on the kernel interpolation, and also incorporated into the in-house version of the open source MPM software Anura3D. The smoothing length in the kernel interpolation depends on the distribution of the original data points. With the cubic spline function, the optimum smoothing length should be between 0.7 and 1.0 times the reference distance between two observed points.

The strategy is used to simulate an experimental rainfall-induced landslide coupling FEM and MPM analysis, thus significantly decreasing the computational cost compared to the sole use of MPM for the entire process. The numerical results agree well with the observations of the experiment.

5 ACKNOWLEDGEMENTS

The authors thank Porf. Matteo Camporese and Prof. Lorenzo Brezzi for the support with the interpretation of the experimental data. Financial support of the University of Padua (BIRD181859) is gratefully acknowledged.

6 REFERENCES

Bandara, S., Ferrari, A., Laloui, L. 2016. Modelling landslides in unsaturated slopes subjected to rainfall infiltration using material point method, *International Journal for Numerical and Analytical Methods in Geomechanics* **40(9)**, 1358–1380.

Ceccato, F., Yerro, A., Girardi, V., Simonini, P. 2021. Two-phase dynamic MPM formulation for unsaturated soil, *Computers and Geotechnics* **129**, 103876.

Fern, J., Rohe, A., Soga, K., Alonso, E. 2019. *The material point method for geotechnical engineering: a practical guide*. CRC Press, Boca Raton, FL.

Gingold, R.A., Monaghan, J.J. 1977. Smoothed particle hydrodynamics: theory and application to non-spherical stars, *Monthly Notices of The Royal Astronomical Society* **181(3)**, 375–389.

Henderson, D., Jacobson, S.H., Johnson, A.W. 2003. The theory and practice of simulated annealing. *Handbook of metaheuristics*, 287–319. Springer, Boston, MA.

Lam, N.S.N. 1983. Spatial interpolation methods: a review, *The American Cartographer* **10(2)**, 129–150.

Lora, M., Camporese, M., Troch, P.A., Salandin, P. 2016. Rainfall-triggered shallow landslides: infiltration dynamics in a physical hillslope model, *Hydrological Processes* **30(18)**, 3239–3251.

Monaghan, J.J., Lattanzio, J.C. 1985. A refined particle method for astrophysical problems, *Astronomy and Astrophysics* **149**, 135–143.

Morgenstern, N.U., Price, V.E. 1965. The analysis of the stability of general slip surfaces, *Geotechnique* **15(1)**, 79–93.

Mühlenstädt, T., Kuhnt, S. 2011. Kernel interpolation, *Computational Statistics & Data Analysis* **55(11)**, 2962–2974.

Soga, K., Alonso, E., Yerro, A., Kumar, K., Bandara, S. 2016. Trends in large-deformation analysis of landslide mass movements with particular emphasis on the material point method, *Géotechnique* **66(3)**, 248–273.

Stanier, S.A., Blaber, J., Take, W.A., White, D.J. 2016. Improved image-based deformation measurement for geotechnical applications, *Canadian Geotechnical Journal* **53(5)**, 727–739.

Van Genuchten, M.T. 1980. A closed-form equation for predicting the hydraulic conductivity of unsaturated soils, *Soil Science Society of America journal* **44(5)**, 892–898.

Wang, B., Vardon, P.J., Hicks, M.A. 2018. Rainfall-induced slope collapse with coupled material point method, *Engineering Geology* **239**, 1–12.

Yerro, A., Girardi, V., Martinelli, M., Ceccato, F. 2022. Modelling unsaturated soils with the Material Point Method. A discussion of the state-of-the-art, *Geomechanics for Energy and the Environment* **32**, 100343.